SAND2019-0317C

Combined computational and experimental study of zirconium tungstate

E. Kim[1,*], M. E. Gordon[2], P. F. Weck[2], J. A. Greathouse[2], S. P. Meserole[2], M. Rodriguez[2], C. Payne[2], C. R. Bryan[2]

[1]*University of Nevada, Las Vegas, NV 89154, USA*
[2]*Sandia National Laboratories, P.O. Box 5800, Albuquerque, NM 87185, USA*

We have investigated cubic zirconium tungstate (ZrW_2O_8) using density functional perturbation theory (DFPT), along with experimental characterization to assess and validate computational results. Cubic zirconium tungstate is among the few known materials exhibiting isotropic negative thermal expansion (NTE) over a broad temperature range, including room temperature where it occurs metastably. Isotropic NTE materials are important for technological applications requiring thermal-expansion compensators in composites designed to have overall zero or adjustable thermal expansion. While cubic zirconium tungstate has attracted considerable attention experimentally, a very few computational studies have been dedicated to this well-known NTE material. Therefore, spectroscopic, mechanical and thermodynamic properties have been derived from DFPT calculations. A systematic comparison of the calculated infrared, Raman, and phonon density-of-state spectra has been made with Fourier transform far-/mid-infrared and Raman data collected in this study, as well as with available inelastic neutron scattering measurements. The thermal evolution of the lattice parameter computed within the quasi-harmonic approximation exhibits negative values below the Debye temperature, consistent with the observed negative thermal expansion characteristics of cubic zirconium tungstate, α-ZrW_2O_8. These results show that this DFPT approach can be used for studying the spectroscopic, mechanical and thermodynamic properties of prospective NTE ceramic waste forms for encapsulation of radionuclides produced during the nuclear fuel cycle.

I. INTRODUCTION

Negative thermal expansion (NTE), occurring in Si and Ge, elemental U, β-quartz, elastomers, some zeolites, and ceramics with framework structures, has been actively investigated experimentally and theoretically for decades owing to its potential applications in high-precision optical systems, nanoscale semiconductor devices, high-performance thermoelectric converters or fuel cells.[1,2,3] While typical NTE materials exhibit anisotropic expansion, that is, contraction in one or two directions coupled with positive thermal expansion in other directions, zirconium tungstate is among the few known materials exhibiting isotropic negative thermal expansion (NTE) over a broad temperature range, including room temperature where it crystallizes in the acentric cubic α-ZrW_2O_8 phase. Isotropic NTE materials are important for technological applications requiring thermal-expansion compensators in composites designed to have overall zero or adjustable thermal expansion. While cubic zirconium tungstate has attracted considerable attention experimentally, a very few computational studies have been dedicated to this well-known NTE material. Here we will discuss about structural and spectroscopic properties including the measured and calculated X-ray Diffraction (XRD) patterns and infrared (IR)/Raman spectra. We have also investigated defects in zirconium tungstate using density functional theory (DFT) to guide ongoing experimental efforts to encapsulate radionuclides into ceramic waste forms.

II. METHODS

First-principles calculations were carried out using DFT, as implemented in the Vienna ab initio simulation package (VASP).[4] The XC energy was calculated using the generalized gradient approximation (GGA), with the PBE [5] parameterization and its PBEsol [6] revised version for solids. Both functionals were found in previous studies to correctly describe the geometric parameters and properties of a variety of Zr compounds and oxides. [7-12] The interaction between valence electrons and ionic cores was described by the projector-augmented wave method. [13-14] The $Zr(4p^6,5s^2,4d^2)$, $W(6s^2,5d^4)$, and $O(2s^2,2p^4)$ electrons were treated explicitly as valence electrons in the Kohn–Sham equations, and the remaining core electrons together with the nuclei were represented by projector-augmented wave pseudopotentials. The Kohn–

Sham equation was solved using the blocked Davidson [15] iterative matrix diagonalization scheme. The plane-wave cutoff energy for the electronic wavefunctions was set to a value of 500 eV, ensuring the total energy of the system to be converged to within 1 meV per atom. Structural optimization was carried out using the α-ZrW_2O_8 crystal structure (space group $P2_13$, IT No. 198; Z = 4) reported by Evans et al.[16] as the initial guess. The Brillouin zone was sampled using the Monkhorst–Pack k-point scheme,[17] with a k-point mesh of 5 × 5 × 5. No symmetry constraints were imposed in unit-cell optimization calculations. Relaxation calculations were first carried out until the Hellmann–Feynman forces acting on atoms were converged within 0.01 eV/Å. Density functional perturbation theory (DFPT) linear response calculations were then carried out at these levels of theory with VASP to determine the vibrational frequencies and associated intensities. The latter were computed based on the Born effective charges (BEC) tensor, which corresponds to the change in atoms polarizabilities with respect to an external electric field. Thermal properties were further derived from phonon calculations within the QHA, which introduces a volume dependence of phonon frequencies as a part of the anharmonic effect

α-ZrW_2O_8 samples were synthesized using a cubic hydrated precursor, $ZrW_2O_7(OH)_2(H_2O)_2$, following the procedure from Closmann et al.,[18] The precursor $ZrW_2O_7(OH)_2(H_2O)_2$ is nearly isostructural with the target α-ZrW_2O_8 phase, which was then heated to 600 °C for 10 hr and allowed to cool to ambient temperature. Experimental details can be found in Weck et al.[19] X-ray Diffraction (XRD) analysis was performed at room temperature using a Bruker D2 Phaser diffractometer. This system was equipped with a sealed-tube X-ray source (Cu K_α radiation, λ = 1.5406 Å) operated at 30 kV and 10 mA. A Ni-filter was employed on the diffracted-beam side of the instrument for suppression of K_β radiation. XRD analysis was performed using the program JADE 9.0 (Materials Data, Inc. Livermore, CA). Infrared spectra were collected at room temperature using a Thermo Scientific Nicolet 6700 Fourier transform infrared (FT-IR) spectrometer and OMNIC 8.3 software suite, with a Spectra Tech Collector II-DRIFTS (diffuse reflectance) and an aluminum mirror as background and blank; powder was placed in a holder and spectra were collected.

III. RESULTS AND DISCUSSION

Fig. 1(a) depicts the scanning electron microscope (SEM) images of the synthesized α-ZrW_2O_8 sample with elongated thin crystalline plates or filiform pointed needles while Fig. 1(b) shows the crystal unit cell of the cubic zirconium tungstate, α-ZrW_2O_8. The space group of the relaxed cubic α-ZrW_2O_8 is $P2_13$ (IT No. 198). There are four formula units in the unit cell ($Z = 4$).

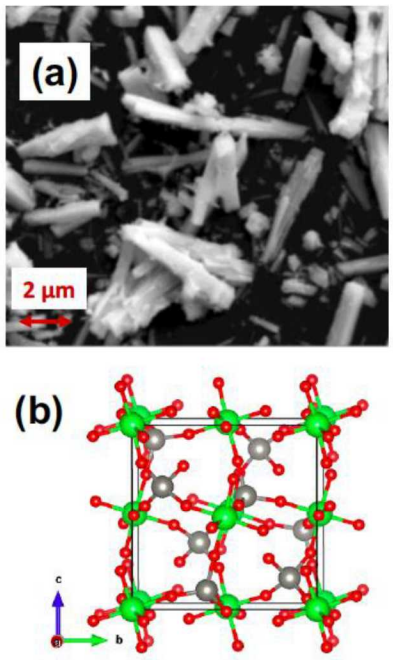

Fig. 1 Synthesized α-ZrW_2O_8 samples: (a) scanning electron microscope (SEM) image and (b) crystal unit cell of α-ZrW_2O_8 (space group $P2_13$, IT No. 198; Z = 4). The green, grey, and red spheres represent Zr, W, and O atoms, respectively.

Fig. 2 illustrates the measured and calculated XRD patterns [see Fig. 2(a)], FTIR [see Fig. 2(b)] and Raman [see Fig. 2(c)] spectra analysis. The observed X-ray diffraction (XRD) patterns of α-ZrW_2O_8 (Cu Kα radiation, λ = 1.5406 Å) and simulated patterns from crystal geometries optimized with DFT at GGA/PBEsol levels of theory indicate that the crystal unit cell parameters of a is 9.241 Å (V = 789.10 Å^3) for GGA/PBEsol and GGA/PBE, respectively, at T = 0 K, which is ~1.0% larger than the present XRD estimate of 9.1493 Å at T = 298 K, due to NTE in the range 0−298 K. The predicted PBEsol lattice parameters reproduce, within ~0.6%, the value of 9.1846 Å refined by Evans et al. at T = 0.3 K using a rigid unit model. It is also found that the predicted PBE lattice parameter is 9.310 Å (V = 806.87 Å^3).

The calculated IR spectrum using PBEsol is overall in excellent agreement with experiment as shown in Fig. 2(b). The IR-active frequency observed by Evans et al. at 646 cm^{-1} (w) and several weak lines in the range 600-400 cm^{-1} (w), which may originate from the formation of ZrO_2 and/or WO_3, were not predicted by DFPT calculations, nor observed in the present experiments.

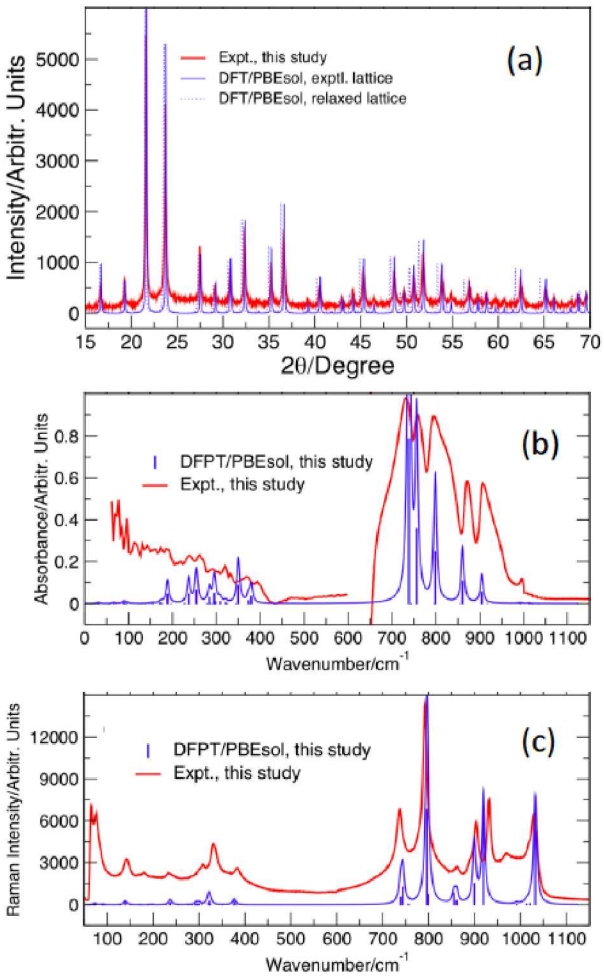

Fig. 2 (a) Observed (red) and calculated (blue) XRD patterns, (b) FT-IR spectrum, and (c) Raman spectrum of α-ZrW_2O_8.

Fig. 2(c) depicts the calculated Raman spectrum with DFPT at the PBEsol levels and the measured Raman-active bands at room temperature in this study, indicating excellent agreement between theory and experiment. No Raman peaks were observed, both theoretically and experimentally, between 400-700 cm^{-1} in this study, implying no formation of ZrO_2 and/or WO_3, in the synthesized ZrW_2O_8 sample, which is consistent with the measured and calculated IR spectra data.

Within the QHA approach, the variations of the linear coefficient of thermal expansion (CTE) of α-ZrW_2O_8 were predicted with DFPT at the GGA/PBE and GGA/PBEsol levels and are depicted in Fig. 3, along with experimental linear CTE estimates extracted from the high-resolution neutron diffraction data of David *et al.* [21]

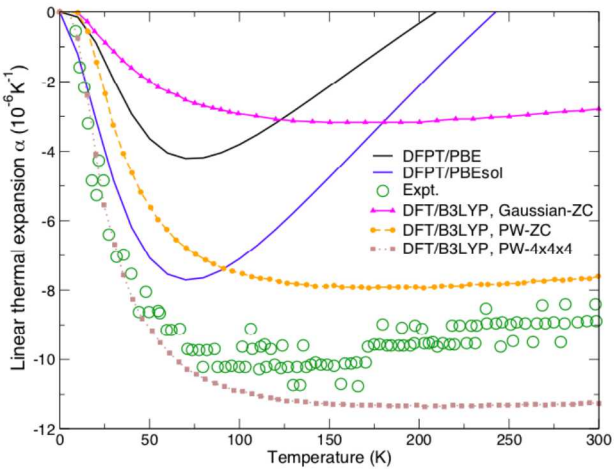

Fig. 3 Linear coefficient of thermal expansion (CTE) of α-ZrW_2O_8 single crystal computed with density functional perturbation theory (DFPT) within the quasi-harmonic approximation (QHA). Scaled DFT predictions by Gava et al. [ref. 20] using the B3LYP hybrid functional with Gaussian-zone-center (ZC), plane-wave (PW) zone-center and PW-(4x4x4) grid approaches within the Debye-Einstein QHA are also displayed in pink, yellow, and brown, respectively. Experimental linear CTE estimates (green circles) is extracted from the high-resolution neutron diffraction data for polycrystalline ZrW_2O_8 (Ref. 21].

As shown in Fig. 3, the negative thermal expansion computed using PBEsol is in very good agreement with experimental data up to ~70 K. Above this temperature, both PBEsol and PBE results exhibit smaller NTE values and, eventually, positive thermal expansion is predicted above 209 K and 243 K with PBE and PBEsol, respectively. While reduction in NTE also appears above ~70 K in the experimental data of David et al.[21] for polycrystalline ZrW_2O_8, computational predictions for single crystal α-ZrW_2O_8 are markedly different from measurements, in the temperature range ~70−300 K. Discrepancies between finite-displacement DFT calculations with the B3LYP hybrid functional and experimental thermal expansion data above ~60 K were also found by Gava et al.[20] These differences may be attributed to the creation of thermally induced defects in real α-ZrW_2O_8 samples, triggering the thermally activated phase transition in cubic ZrW_2O_8, which occurs around 431 K. [22] Such a low-temperature defect creation scenario is plausible owing to the metastable character of α-ZrW_2O_8, which is only thermodynamically stable in a narrow temperature range around 1400 K.

The excellent agreement between theory and experiments indicates that the same DFT framework at the GGA/PBE and GGA/PBEsol levels can be used to investigate the formation of defects in zirconium tungstate.

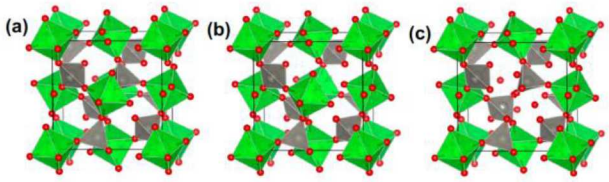

Fig. 4 Crystal unit cells of (a) pristine α-ZrW_2O_8; two possible vacancies: (b) V(W) and (c) V(Zr). Colour legend: Zr, green; W, grey; O, red.

Two different types of vacancies in bulk α-ZrW_2O_8 are considered in this study, denoted as V(Zr) and V(W) when V(Zr) and V(W) represent vacancies at Zr and W sites, respectively. The optimized unit cells for those configurations, along with pristine α-ZrW_2O_8, are shown in Fig. 4 and associated defect formation energies calculated using the GGA/PBE level of theory are listed in Table 1.

Table 1 Defect formation energies in α-ZrW_2O_8. V(Zr) and V(W) represent vacancies at Zr and W sites, respectively.

Type	sites	Defect formation energy (eV)
Vacancies	V(Zr)	28.40
	V(W)	28.73

Further investigation is necessary to examine the possible scenarios of radionuclides encapsulation into zirconium tungstate, ZrW_2O_8. Therefore, ongoing computational efforts include carrying out DFT calculations to evaluate the defect formation energy of substitutional impurities such as S(Zr) and S(W). In this case S(Zr) and S(W) represent the defects when radionuclides substituting Zr and W sites, respectively.

III. CONCLUSIONS

Density functional perturbation theory (DFPT) has been used to investigate structural, vibrational, and thermal properties of cubic zirconium tungstate. A systematic comparison of the calculated infrared and Raman spectra has been made with Fourier transform far-/mid-infrared and Raman data collected, showing excellent agreement between theory and experiments. The theoretically predicted variations of the linear coefficient of thermal expansion (CTE) of cubic ZrW_2O_8 using DFPT at the GGA/PBE and GGA/PBEsol levels are compared with experimental linear CTE estimates extracted from the high-resolution neutron diffraction data. The calculated negative thermal expansion is in very good agreement with experimental data up to ~70 K. These results show that this DFPT approach can serve as a valuable tool to study the spectroscopic and thermo-mechanical properties of prospective NTE ceramic waste forms for encapsulation of radionuclides produced during the nuclear fuel cycle.

ACKNOWLEDGMENTS

Sandia National Laboratories is a multimission laboratory managed and operated by National Technology and Engineering Solutions of Sandia LLC, a wholly owned subsidiary of Honeywell International Inc. for the U.S. Department of Energy's National Nuclear Security Administration under contract DE-NA0003525. This work was performed, in part, at the Center for Integrated Nanotechnologies, an Office of Science User Facility operated for the U.S. Department of Energy (DOE) Office of Science by Sandia National Laboratories (Contract DE-NA-0003525).

REFERENCES

1. Sleight, A. W. Isotropic Negative Thermal Expansion. *Ann. Rev. Matter. Sci.* **1998**, *28*, 29–43
2. Evans, J. S. O. Negative Thermal Expansion Materials. *J. Chem. Soc. Dalton Trans.* **1999**, 3317–3326.
3. Takenaka, K. Negative Thermal Expansion Materials: Technological Key for Control of Thermal Expansion. *Sci. Technol. Adv. Mater*. **2012**, *13*, 013001.
4. Kresse, G.; Furthmüller, J. Efficient Iterative Schemes for Ab Initio Total-Energy Calculations Using a Plane-Wave Basis Set. *Phys. Rev.* B **1996**, *54*, 11169-11186.
5. Perdew, J. P.; Burke, K.; Ernzerhof, M. Generalized Gradient Approximation Made Simple. *Phys. Rev. Lett.* **1996**, *77*, 3865-3868.
6. Perdew, J. P.; Ruzsinszky, A.; Csonka, G. I.; Vydrov, O. A.; Scuseria, G. E.; Constantin, L. A.; Zhou, X.; Burke, K. Restoring the Density-Gradient Expansion for Exchange in Solids and Surfaces. *Phys. Rev. Lett.* **2008**, *100*, 136406.
7. Weck, P. F.; Kim, E. Assessing Hubbard-Corrected AM05+U and PBEsol+U Density Functionals for Strongly Correlated Oxides CeO_2 and Ce_2O_3. *Chem. Phys. Phys. Chem*. **2016**, *18*, 26816-26826.
8. Weck, P. F.; Kim, E. Uncloaking the Thermodynamics of the Studtite to Metastudtite

Shear-Induced Transformation. *J. Phys. Chem. C* **2016**, *120*, 16553-16560.
9. Weck, P. F.; Kim, E.; Tikare, V.; Mitchell, J. A. Mechanical Properties of Zirconium Alloys and Zirconium Hydrides Predicted from Density Functional Perturbation Theory. *Dalton Trans*. **2015**, *44*, 18769-18779.
10. Weck, P. F.; Kim E. Layered Uranium(VI) Hydroxides: Structural and Thermodynamic Properties of Dehydrated Schoepite α-$UO_2(OH)_2$. *Dalton Trans.* **2014**, *43*, 17191.
11. Weck, P. F.; Kim E. Solar Energy Storage in Phase Change Materials: First-Principles Thermodynamic Modeling of Magnesium Chloride Hydrates. *J. Phys. Chem. C* **2014**, *118*, 4618.
12. Weck, P. F.; Juan, P.-A.; Dingreville, R.; Kim, E. Density Functional Analysis of Fluorite-Structured $(Ce,Zr)O_2/CeO_2$ Interfaces. *J. Phys. Chem. C* **2017**, *121*, 14678.
13. Blöchl, P. E. Projector Augmented-Wave Method. *Phys. Rev.* B **1994**, *50*, 17953-17979.
14. Kresse, G.; Joubert, D. From Ultrasoft Pseudopotentials to the Projector Augmented-Wave Method. *Phys. Rev.* B **1999**, *59*, 1758-1775.
15. Davidson, E. R. *Methods in Computational Molecular Physics*, G. H. F. Diercksen and S. Wilson, Eds., Vol. 113, NATO Advanced Study Institute, Series C, Plenum, New York, 1983, p. 95.
16. Evans, J. S. O.; David, W. I. F., Sleight, A. W. Structural Investigation of the Negative-Thermal-Expansion Material ZrW_2O_8. *Acta Crystallogr.B* **1999**, *55*, 333-340.
17. Monkhorst, H. J.; Pack, J. D. Special Points for Brillouin-Zone Integrations. *Phys. Rev.* B **1976**, *13*, 5188-5192.
18. Closmann, C.; Sleight, A. W.; Haygarth, J. C. Low-Temperature Synthesis of ZrW_2O_8 and Mo-Substituted ZrW_2O_8. *J. Sol. State Chem*. **1998**, *139*, 424-426.
19. Weck, P. F.; Kim, E., Greathouse, J. A., Gordon, M. E. Gordon, Bryan, C. R., Assessing exchange-correlation functionals for elasticity and thermodynamics of α-ZrW2O8: A density functional perturbation theory study, Chemical Physics Letters, 698, 2018, 195-199.
20. Gava, V.; Martinotto, A. L.; Perottoni, C. A. First-Principles Mode Grüneisen Parameters and Negative Thermal Expansion in α-ZrW_2O_8. *Phys. Rev. Lett*. **2012**, *109*, 195503.
21. David, W. I. F.; Evans, J. S. O.; Sleight, A. W. Direct Evidence for a Low-Frequency Phonon Mode Mechanism in the Negative Thermal Expansion Compound ZrW_2O_8. *Europhys. Lett.* **1999**, *46*, 661-666.
22. Evans, J. S. O.; Mary, T. A.; Vogt, T.; Subramanian, M. A.; Sleight, A. W. Negative Thermal Expansion in ZrW_2O_8 and HfW_2O_8. *Chem. Mater.* **1996**, *8*, 2809-2823.